Open access • Journal Article • DOI:10.1021/ACS.INORGCHEM.8B00021

Theoretical Prediction and Synthesis of (Cr2/3Zr1/3)2AlC i-MAX Phase.

Liugang Chen, Martin Dahlqvist, Thomas Lapauw, Bensu Tunca ...+7 more authors

Institutions: Katholieke Universiteit Leuven, Linköping University

Published on: 11 May 2018 - Inorganic Chemistry (American Chemical Society)

Topics: Phase (matter), Monoclinic crystal system, Crystal structure, Stoichiometry and Chemical composition

Theoretical prediction and synthesis of $(Cr_{2/3}Zr_{1/3})_2AlC$ *i*-MAX phase

Liugang Chen[1†*], Martin Dahlqvist[2†], Thomas Lapauw[1,3], Bensu Tunca[1,3], Fei Wang[1], Jun Lu[2], Rahele Meshkian[2], Konstantina Lambrinou[3], Bart Blanpain[1], Jozef Vleugels[1], Johanna Rosen[2*]

[1]KU Leuven, Department of Materials Engineering (MTM), Kasteelpark Arenberg 44, B-3001 Leuven, Belgium
[2]Department of Physics, Chemistry, and Biology (IFM), Linköping University, SE-581 83 Linköping, Sweden
[3]SCK•CEN, Boeretang 200, B2400 Mol, Belgium

[†]L. Chen and M. Dahlqvist contributed equally to this work
* Corresponding authors. Email: liugang.chen@kuleuven.be (L.C.) and johanna.rosen@liu.se (J.R.)

Notes The authors declare that there is no competing financial interest.

Keywords

MAX phase Ceramics; Solid solution MAX phases; Ordered MAX phases; Hot pressing; X-ray diffraction

Abstract

Guided by predictive theory, a new compound with chemical composition $(Cr_{2/3}Zr_{1/3})_2AlC$ was synthesized by hot pressing of Cr, ZrH_2, Al and C mixtures at 1300°C. The crystal structure is monoclinic of space group *C*2/*c* and displays in-plane chemical order in the metal layers, a so-called *i*-MAX phase. Quantitative chemical composition analyses confirmed that the primary phase had a $(Cr_{2/3}Zr_{1/3})_2AlC$ stoichiometry, with secondary Cr_2AlC, $AlZrC_2$ and ZrC phases and a small amount of Al-Cr intermetallics. A theoretical evaluation of the $(Cr_{2/3}Zr_{1/3})_2AlC$ magnetic structure was performed, indicating an antiferromagnetic ground state. Also $(Cr_{2/3}Hf_{1/3})_2AlC$, of the same structure, was predicted to be stable.

Introduction

MAX phases are a group of nanolayered, hexagonal phases, with the general formula of $M_{n+1}AX_n$ (n = 1, 2, or 3), in which ‘‘M’’ ‘‘A’’ and ‘‘X’’ are an early transition metal, an A-group element, and C and/or N, respectively[1]. Because of their nanolayered structure some MAX phases, especially Al-containing MAX compounds[1,2], have combined characteristic properties of both ceramics and metals, for example excellent corrosion and oxidation resistances at elevated temperatures, and easy machinability. Thanks to these properties, such MAX phases are

potential materials for the accident-tolerant fuel cladding used in the light water reactors where the materials are commonly exposed to mechanical and thermal loading, high neutron irradiation and oxidation[3,4]. To date, over 70 MAX phases have been synthesized experimentally[1]. Among these MAX phases, Zr-Al-C MAX ceramics, *i.e.* Zr_3AlC_2 and Zr_2AlC[3,4], which were recently synthesized , are considered as promising candidates for fuel cladding coatings, due to the small cross-section of Zr for neutrons[5]. However, prior studies illustrate that other MAX phase-like carbides in the Zr-Al-C ternary system, *e.g.* $Zr_2Al_3C_4$ and $Zr_2[Al(Si)]_4C_5$, exhibit a poor oxidation resistance[6,7], because the formed Al_2O_3 and ZrO_2 oxide scales are non-protective[6,7]. Most probably, the oxidation resistance of Zr_3AlC_2 and Zr_2AlC MAX phases is also modest. On the other hand, similar studies conducted in the oxidation behavior of $Zr_2(AlSi)_4C_5$ ceramics doped with titanium (Ti) implied that the oxidation resistance is improved because of the addition of titanium[8]. Therefore, MAX phases in the Ti-Zr-Al-C system, *i.e.* $(Ti,Zr)_2AlC$, and $(Ti_{0.67},Zr_{0.33})_3AlC_2$, have been recently synthesized[9], because $Ti_{n+1}AlC_n$ MAX phases, *i.e.* Ti_2AlC and Ti_3AlC_2, are also recognized as promising materials for the nuclear fuel cladding. Cr_2AlC is another promising candidate based on the excellent oxidation and hot corrosion resistance and low neutron absorption cross-section[1,2,5]. From the neutron cross-section point of view, the substitution of Cr in a Cr_2AlC MAX phase by Zr would be of high interest, thereby generating new MAX phases in the Cr-Zr-Al-C system. However, theoretical predictions based on the energy of mixing data and density of states analysis indicated that $(Cr_{1-x},Zr_x)_2AlC$ phases with varying x were unstable[10]. Recent attempts in the synthesis of $(Cr_{1-x},Zr_x)_2AlC$ MAX phases were also reported to be unsuccessful[5]. So far, MAX phases in the Cr-Zr-Al-C system have not been reported theoretically nor experimentally. However, recent reports of in-plane chemically ordered quaternary MAX phases (*i*-MAX) with a 2:1 ratio of the two metals, e.g., $(Mo_{2/3}Sc_{1/3})_2AlC$[11], $(Cr_{2/3}Sc_{1/3})_2AlC$[12], $(V_{2/3}Zr_{1/3})_2AlC$ and $(Mo_{2/3}Y_{1/3})_2AlC$[13] inspired our interest for the $(Cr_{2/3}Zr_{1/3})_2AlC$ phase synthesis. In this study, we therefore reexamine the Cr-Zr-Al-C system based on the recent discoveries of *i*-MAX phases. Guided by theoretical predictions, showing $(Cr_{2/3}Zr_{1/3})_2AlC$ to be stable, we successfully synthesized $(Cr_{2/3}Zr_{1/3})_2AlC$.

Method

Theoretical details

All first-principles calculations based on density functional theory were performed with the Vienna *ab-initio* simulation package (VASP)[14–16] using the projector augmented wave method[17,18] with spin-polarized generalized gradient approximation (GGA) as parameterized by Perdew-Burke-Ernzerhof (PBE)[19] for treating electron exchange

and correlation effects. Wave functions were expanded in plane waves up to an energy cutoff of 400 eV, and sampling of the Brillouin zone were done using the Monkhorst-Pack scheme[20]. In addition, we also used the rotationally invariant approach as proposed by Dudarev[21]. Note that within this formalism the onsite Coulomb parameter U and the exchange parameter J are spherically averaged into a single effective interaction parameter $U_{\text{eff}} = U - J$ which does not depend on their individual values. The equilibrium structures are obtained by minimization of the total energy with respect to volume and with full relaxation of atomic positions and unit cell parameters until forces are converged below 10^{-3} eV Å^{-1}.

We have considered several collinear magnetic spin configurations for $\left(\mathrm{Cr}_{2/3}M^2_{1/3}\right)_2\mathrm{AlC}$, M^2 = Ti, Zr, or Hf, whose notation are familiar with those defined previously for M_2AX phases in general[22–24]. Table 1 summarizes the applied spin direction at each Cr site in the monoclinic $C2/c$ (#15) unit cell for each corresponding spin configuration, and Figure 1 shows a schematic representation of the enumeration of Cr sites. For simplicity, we use a shortened version for some notations; AFM1 = $\mathrm{AFM}[001]_1$, X2 = $\mathrm{AFM}[001]^X_2$, A2 = $\mathrm{AFM}[001]^A_2$, and in-A = in-AFM (i.e. in-plane ordered AFM spin configurations with 2 up and 2 down spins on M^1 in each layer). All considered spin configurations are visualized in Figure S1.

Table 1. Definition of eight magnetic spin configurations considered for $\left(\mathrm{Cr}_{2/3}M^2_{1/3}\right)_2\mathrm{AlC}$, M^2 = Ti, Zr, or Hf, within the monoclinic Bravais unit cell of space group $C2/c$ consisting of 48 atoms where the 16 Cr atoms occupy two different 8f Wyckoff sites. For simplicity, we use shortened version for some notations; AFM1 = $\mathrm{AFM}[001]_1$, X2 = $\mathrm{AFM}[001]^X_2$, A2 = $\mathrm{AFM}[001]^A_2$, and in-A = in-AFM (i.e. in-plane ordered AFM spin configurations).

site	number	Direct coordinate			Spin configuration							
		x	y	z	FM	AFM1	X2	A2	in-A1	in-A2	in-A3	in-A4
Cr1	1	x	y	z	+	+	+	+	-	-	-	+
Cr1	2	x+1/2	y+1/2	z	+	+	+	+	-	-	-	+
Cr2	3	x	y	z	+	+	+	+	+	+	+	-
Cr2	4	x+1/2	y+1/2	z	+	+	+	+	+	+	+	-
Cr1	5	-x	y	-z+1/2	+	-	+	-	-	-	+	-
Cr1	6	-x+1/2	y+1/2	-z+1/2	+	-	+	-	-	-	+	-
Cr2	7	-x	y	-z+1/2	+	-	+	-	+	+	-	+
Cr2	8	-x+1/2	y+1/2	-z+1/2	+	-	+	-	+	+	-	+
Cr1	9	x	-y	z+1/2	+	+	-	-	+	-	+	+
Cr1	10	x+1/2	-y+1/2	z+1/2	+	+	-	-	+	-	+	+
Cr2	11	x	-y	z+1/2	+	+	-	-	-	+	-	-
Cr2	12	x+1/2	-y+1/2	z+1/2	+	+	-	-	-	+	-	-
Cr1	13	-x	-y	-z	+	-	-	+	+	-	-	-
Cr1	14	-x+1/2	-y+1/2	-z	+	-	-	+	+	-	-	-

Cr2	15	-x	-y	-z	+	-	-	+	-	+	+	+
Cr2	16	-x+1/2	-y+1/2	-z	+	-	-	+	-	+	+	+

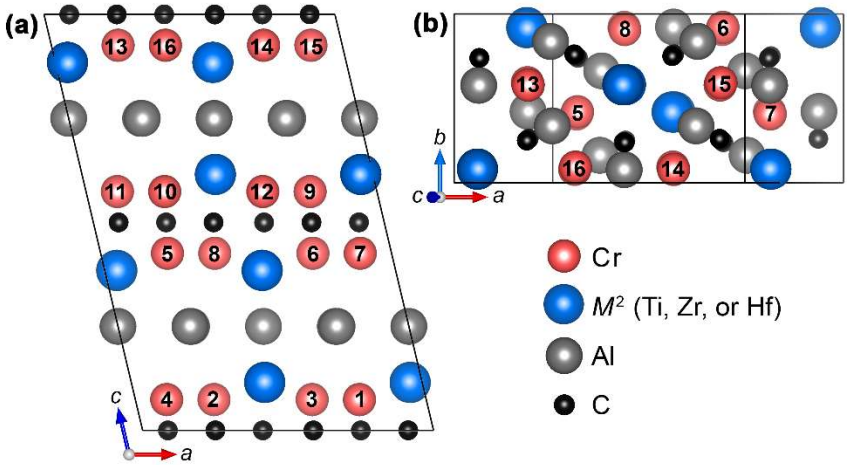

Fig. 1. Schematic of the monoclinic $C2/c$ $\left(Cr_{2/3}M^2_{1/3}\right)_2AlC$, M^2 = Ti, Zr, or Hf along the (a) [010] and (b) [103] zone axis with enumeration of Cr atoms. Schematics were produced with VESTA[25].

The thermodynamic stability was evaluated using a linear optimization procedure based on the simplex method, which compares the energy of the compound of interest to all possible linear combinations of other competing phases under the constraint of a fixed stoichiometry[26,27]. Temperature dependent effects such as lattice vibrations were not considered, as such contribution from a phase, significant or not, tend to be cancelled out in the calculated stability[28]. This approach has been proven to work exceptionally well for both MAX[27,29,30] and *i*-MAX phases[11,13]. The linear combination of competing phases resulting in the lowest energy is called equilibrium simplex or set of most competing phases. A compound's stability can be quantified in terms of formation enthalpy ΔH_{cp} by comparing its energy to the energy of the equilibrium simplex, $\Delta H_{cp} = E(\text{compound}) - E(\text{equilibrium simplex})$. If $\Delta H_{cp} < 0$ the compound is considered stable, while for $\Delta H_{cp} > 0$ it is considered to be not stable or at best metastable. For a compound found not stable, the equilibrium simplex indicates which other phases are more stable. Competing phases included in the evaluation of phase stability are those experimentally known as well as hypothetical phases that exist in similar and/or with neighboring elements in the Periodic table of elements. A complete list of competing phases considered herein for the Cr-*M*-Al-C systems, where *M* = Ti, Zr, and Hf, is given in Table S1 in the supporting information.

Chemical disorder, or solid solution, of Cr and M^2 were modelled using the special-quasi random structures (SQS) method[31] using cell sizes up to 6×4×1 unit cells. It is possible to estimate the temperature required to lower the energy of the disordered phases to the ordered phases, through entropic contribution ΔS to the free energy, using

$$T_{disorder} = \frac{\Delta H_{cp}^{disorder} - \Delta H_{cp}^{order}}{\Delta S}, \quad (1)$$

for which $\Delta G_{cp}^{disorder}[T] = \Delta H_{cp}^{order}$ is fulfilled and hence give an estimate above which temperature disorder is expected.

Experimental details

The starting powders were Cr (> 99% purity, particle size < 40 μm, Baudier, France), ZrH_2 (>99% purity, particle size <6 μm, Chemetall, Germany), Al (>99% purity, particle size <5 μm, AEE, US) and C (>99% purity, particle size <5 μm, Asbury Graphite Mills, US). ZrH_2 was used because of our previous experience in the preparation of Zr-containing MAX phases[3,4,9]. So far, we have not been able to prepare Zr-based MAX phases starting from Zr powder, implying the use of ZrH_2 is essential. The powders were mixed in four different Cr:Zr:Al:C molar ratios of (2-2x):2x:1.1:0.95 (x =0.2, 0.33, 0.32 and 0.5), denoted as Z20, Z33, Z32 and Z50 respectively, with a (Cr+Zr):Al:C molar ratio of 2:1.1:0.95. The excess of Al was used to compensate for its loss during high temperature processing and a sub-stoichiometric C was considered because of the inward diffusion of C from the surrounding graphite die/punch set-up during hot pressing, as commonly reported in literature[3,4,9].

The starting powder mixtures were dry mixed under Ar atmosphere on a Turbula multidirectional mixer in polyethylene containers for 24h. Five millimeter diameter ZrO_2 milling balls (Grade TZ-3Y, Tosoh, Japan) were added in a ball-to-powder weight ratio of 3:1 to break up agglomerates and mix the powders. After mixing for 24h, the formation of alloys or decomposition of ZrH_2 did not occur, as indicated by the XRD pattern of the mixed powders of sample Z02, shown in Fig. S2. The mixed powders were sieved and uniaxially pre-compacted in a 30 mm diameter graphite die at 30 MPa. The powder loaded graphite die/punch set-up was then hot pressed (HP, W100/150-2200-50 LAX, FCT Systeme, Frankenblick, Germany) for 30 min at 1100-1400°C in an actively pumped vacuum (~10 Pa) under a pressure of 30 MPa with a heating rate of 20°C/min and natural cooling. The discs were sand blasted to remove the graphite paper and an additional 200 μm were ground off by SiC grinding paper to

remove the outer carbide reaction layer. Diamond paste polished surfaces were used for XRD, SEM and EPMA analysis.

The phase composition of the as-prepared ceramics was obtained by XRD (D2, Bruker, Germany) using Cu Kα radiation at 30 kV and 10 mA. The phase content was attained with a step size of 0.01° and a time of 0.5 s per step. The lattice parameters of related phases were calculated via Rietveld refinement using the Materials Analysis Using Diffraction (MAUD) software[32], and were employed to generate the powder diffraction pattern of $(Cr_{2/3}Zr_{1/3})_2AlC$ compound by Powder Cell software[33].

Compositional analyses were performed to determine the Cr:Zr:Al:C molar ratio, with a full quantitative electron probe X-ray micro-analyser coupled with wavelength dispersive spectroscopy (EPMA-WDS, JXA-8530F, JEOL Ltd.) using standards. The elemental distribution of Cr, Zr, Al, and C in the hot pressed ceramics was mapped with EPMA-WDS. The EPMA-WDS was operated using a probe current of 15 nA and an acceleration voltage of 15 kV . Microstructural analyses were done on a scanning electron microscope (SEM, XL30-FEG, FEI) at 15 kV. The Vickers hardness (FV-700, Future-Tech Corp., Tokyo, Japan) was measured using an indentation load of 3 kg with a dwell time of 10 s on a well-polished surface. The reported value is the average of five indents.

Scanning transmission electron microscopy (STEM) combined with high angle annular dark field imaging (STEM-HAADF) was performed in the double-corrected Linköping FEI Titan3 60-300, operated at 300 kV. Selected area electron diffraction (SAED) was performed on a FEI Tecnai T20 TEM operated at 200 kV. The specimens were prepared by directly dispersing the ground-mixed powder in a Cu grid with holey C film.

Results and discussion

Theoretical predictions

Theoretical phase stability calculations for $\left(Cr_{2/3}M^2_{1/3}\right)_2AlC$, M^2 = Ti, Zr, or Hf, in a monoclinic $C2/c$ structure with the in-plane chemically ordering were firstly started. This structure is closely related to the ternary M_2AX phase, where Cr_2AlC, Ti_2AlC, and Zr_2AlC are experimentally known. For the stability evaluation, it is important to consider possible formation of other competing phases within each quaternary system. A complete list of competing phases is shown in Fig. S1. The phase stability prediction of $(Cr_{2/3}Ti_{1/3})_2AlC$, $(Cr_{2/3}Zr_{1/3})_2AlC$ and $(Cr_{2/3}Hf_{1/3})_2AlC$ is summarized in Table 2. All are found with a formation enthalpy $\Delta H_{cp} < 0$, thus indicating they are stable. However,

one important aspect is to also consider possible formation of a solid solution of Cr and M^2 in the M_2AX structure. We do this by comparing the energy of ordered structures with those where Cr and M^2 are in a solid solution on the M lattice. This energy difference is then transferred into a disorder temperature T_{disorder}, i.e., temperature required to favor the disordered structure due to configurational entropy, using Eq. 1. Only $(Cr_{2/3}Zr_{1/3})_2AlC$ and $(Cr_{2/3}Hf_{1/3})_2AlC$ have T_{disorder} well above a typical bulk synthesis temperature ~1500 °C (1773 K). In summary, from ΔH_{cp} and T_{disorder} we conclude that $(Cr_{2/3}Zr_{1/3})_2AlC$ is most likely to form an ordered *i*-MAX phase whereas a solid solution is expected for $(Cr_{2/3}Ti_{1/3})_2AlC$. The latter conclusion is supported by experimental reports for similar systems[13,34].

Table 2. Calculated formation enthalpy ΔH_{cp}, equilibrium simplex, and disorder temperature T_{disorder} for $(Cr_{2/3}Ti_{1/3})_2AlC$, $(Cr_{2/3}Zr_{1/3})_2AlC$ and $(Cr_{2/3}Hf_{1/3})_2AlC$

Phase	equilibrium simplex (most competing phases)	ΔH_{cp} (meV/atom)	T_{disorder} (K)
$(Cr_{2/3}Ti_{1/3})_2AlC$	$TiCr_2AlC_2$ (o-MAX), Cr_2Al, $TiAl_3$, TiC	-16	1598
$(Cr_{2/3}Zr_{1/3})_2AlC$	ZrC, Cr_2AlC, Cr_2Al, $ZrAl_3$	-58	7574
$(Cr_{2/3}Hf_{1/3})_2AlC$	HfC, Cr_2AlC, Cr_2Al, Cr_5Al_{21}	-24	6460

Material synthesis and structural determination

Based on theoretical predictions showing $(Cr_{2/3}Zr_{1/3})_2AlC$ and $(Cr_{2/3}Hf_{1/3})_2AlC$ to be stable and with a high disorder temperature (well above typical bulk synthesis conditions), we focussed our synthesis attempts on the $(Cr_{2/3}Zr_{1/3})_2AlC$ phase. XRD patterns of the Z20 ceramic after hot pressing for 30 min at 1100-1400°C are shown in Fig. 2a. ZrC, Cr_7Cr_3 and Zr-Al and Cr-Al intermetallics are the main phases of the ceramic synthesised at 1100°C. The ceramic processed at 1200°C contains Cr_2AlC MAX phase, ZrC, Al-Cr intermetallic and an unidentified peak at $2\theta = 40.42°$ are observed. When hot-pressed at 1300°C ZrC, Cr_2AlC, $AlZrC_2$ and Al_8Cr_5 are formed along with a series of peaks that belongs to the *i*-MAX phase $(Cr_{2/3}Zr_{1/3})_2AlC$, which have similar positions as $Zr_3Al_3C_5$ and $AlZrC_2$[35,36]. Upon increasing the temperature to 1400°C, these peaks totally disappeared, whereas the peaks belonging to $AlZrC_2$, such as at $2\theta = 6.7°$, remained.

Figure 2b shows the XRD patterns of the hot-pressed Cr, ZrH_2, Al and C mixtures with different primal Cr:Zr:Al:C molar ratios, but an identical overall (Cr+Zr):Al:C molar ratio of 2:1.1:0.95. ZrC, Cr_2AlC and $AlZrC_2$ are observed in the Z20 and Z33 ceramics, and ZrC and Cr_2AlC are found in the Z32 ceramic. The series of peaks that belongs to $(Cr_{2/3}Zr_{1/3})_2AlC$ (at for example $2\theta = 40.42°$) are observed in Z20, Z33 and Z32, but not in Z50. Comparing Z33 and

Z32 ceramics reveals that the $AlZrC_2$ (2θ = *6.7*°) phase completely disappears (as shown in Fig. 3), whereas the $(Cr_{2/3}Zr_{1/3})_2AlC$ peak at 2θ = *40.42*° is present in the Z32 ceramic with a slightly decreased Zr content. Therefore, it can be concluded that these peaks correspond to the same compound, i.e., $(Cr_{2/3}Zr_{1/3})_2AlC$. Upon further increasing the Zr content (Z50 ceramic), ZrC is the predominant phase with a trace amount of Cr_2AlC. This is probably because Zr readily reacts with C and the Zr:C molar ratio is 1:0.95 in Z50, implying most of the C was consumed to form ZrC. As a result, Al and Cr were remained and partially exuded in liquid form from the die/punch system during hot pressing. In fact, Cr_2AlC and Al_4C_3 were found on the surface of the graphite die and punch (not shown here).

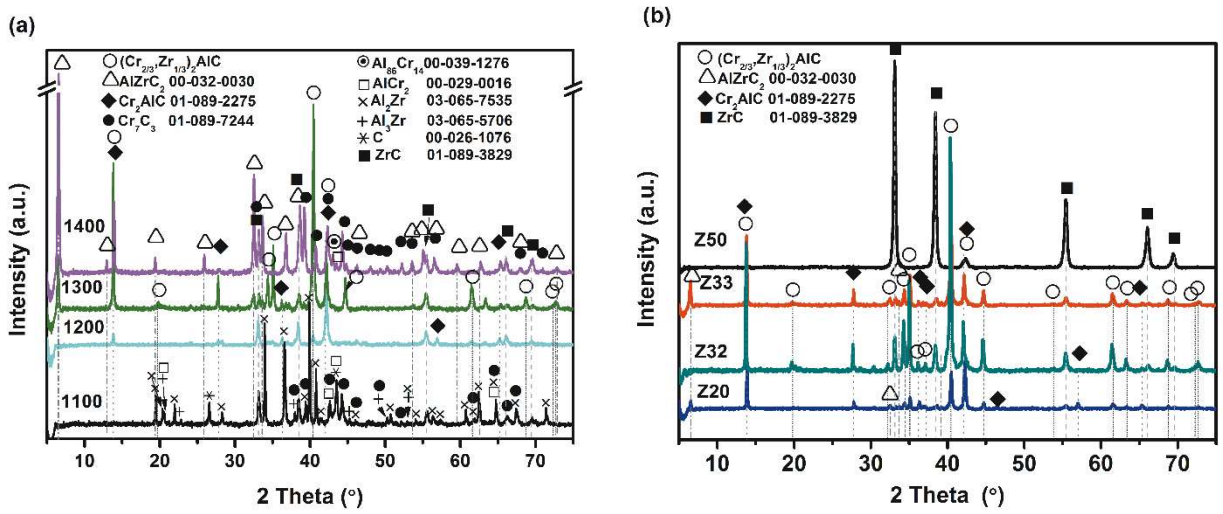

Fig. 2. XRD patterns of (a) the Z20 ceramic hot pressed for 30 min at 1100, 1200, 1300 and 1400°C, and (b) the ceramics with different initial Cr:Zr:Al:C molar ratios, hot-pressed for 30 min at 1300°C.

The refined XRD pattern of the Z32 ceramic based on $(Cr_{2/3}Zr_{1/3})_2AlC$ with space group C2/c is shown in Fig. 3. The Rietveld refinement reveals that the majority of the sample consist of $(Cr_{2/3}Zr_{1/3})_2Al$, 84.8 ± 1.7 wt%, with minor inclusion of 5.8 ± 0.5 wt% Cr_2AlC and 9.4 ± 0.00 wt% ZrC. The *a*, *b*, and *c* lattice constants and angle β of the $(Cr_{2/3}Zr_{1/3})_2AlC$ compound, as determined by XRD, are 9.0595 ± 0.0007 Å, 5.2256 ± 0.0003 Å, 13.2378 ± 0.0007 Å, and 103.2459 ± 0.01 °. Both the theoretical calculation and Rietveld analysis indicate the crystal structure of $(Cr_{2/3}Zr_{1/3})_2AlC$ is monoclinic with a *C*2/*c* symmetry.

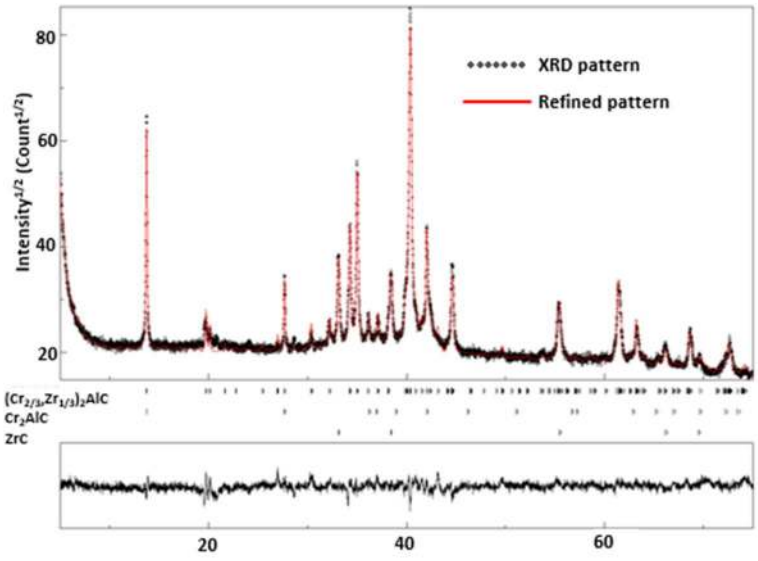

Fig. 3. The XRD pattern (black) and refinement (red) of the Z32 ceramic.

The d-spacings and corresponding 2θ values of (*hkl*) reflections, as calculated for the powder diffraction pattern of $(Cr_{2/3}Zr_{1/3})_2AlC$, are shown in Table S2. Due to the low intensities and overlapping peaks (Fig. 3), most of the 2θ values could not be resolved in the experimental pattern. However, the experimentally measured and theoretical 2θ values for the clearly identifiable diffraction peaks are comparable.

Fig. 4 demonstrates the backscattered electron (BSE) images of Z20, Z33, and Z32 ceramics after hot-pressing. As shown in Fig. 4a and 4b, four different phases can be differentiated by backscattered electron (BSE) contrast in Z20 and Z33 after hot pressing at 1300°C. In order to assist in identifying these phases, EPMA-WDS elemental mapping was performed on the marked area in Fig. 4a, as shown in Fig. 5. The Cr_2AlC, $AlZrC_2$ and ZrC phases appear dark-grey, grey and white, respectively, under BSE contrast in Fig. 4a and 4b. The large grained light grey contrast phase in the right-upper corner of the insert in Fig. 4a consists of Cr, Zr, Al and C, see Fig. 5, confirming the formation of the $(Cr_{2/3}Zr_{1/3})_2AlC$ compound in the Cr-Zr-Al-C system. As shown in Fig. 4a, the Z20 ceramic contains large agglomerates with a grain size of 1-200 µm surrounded by $AlZrC_2$. When the temperature increases to 1400°C, only small grained $AlZrC_2$ with a rectangular shape, ZrC and Cr_7C_3 are observed in the Z20 ceramic (Fig. 4d). Note that no $AlZrC_2$ phase is formed in the Z32 ceramic (Fig. 4c). The bright grey $(Cr_{2/3}Zr_{1/3})_2AlC$ phase has a pronounced volume fraction in this ceramic, whereas the amount of dark-grey Cr_2AlC MAX phase and white ZrC phase is less (Fig. 4c). These SEM observations are consistent with the quantification of the XRD pattern (Fig. 2b).

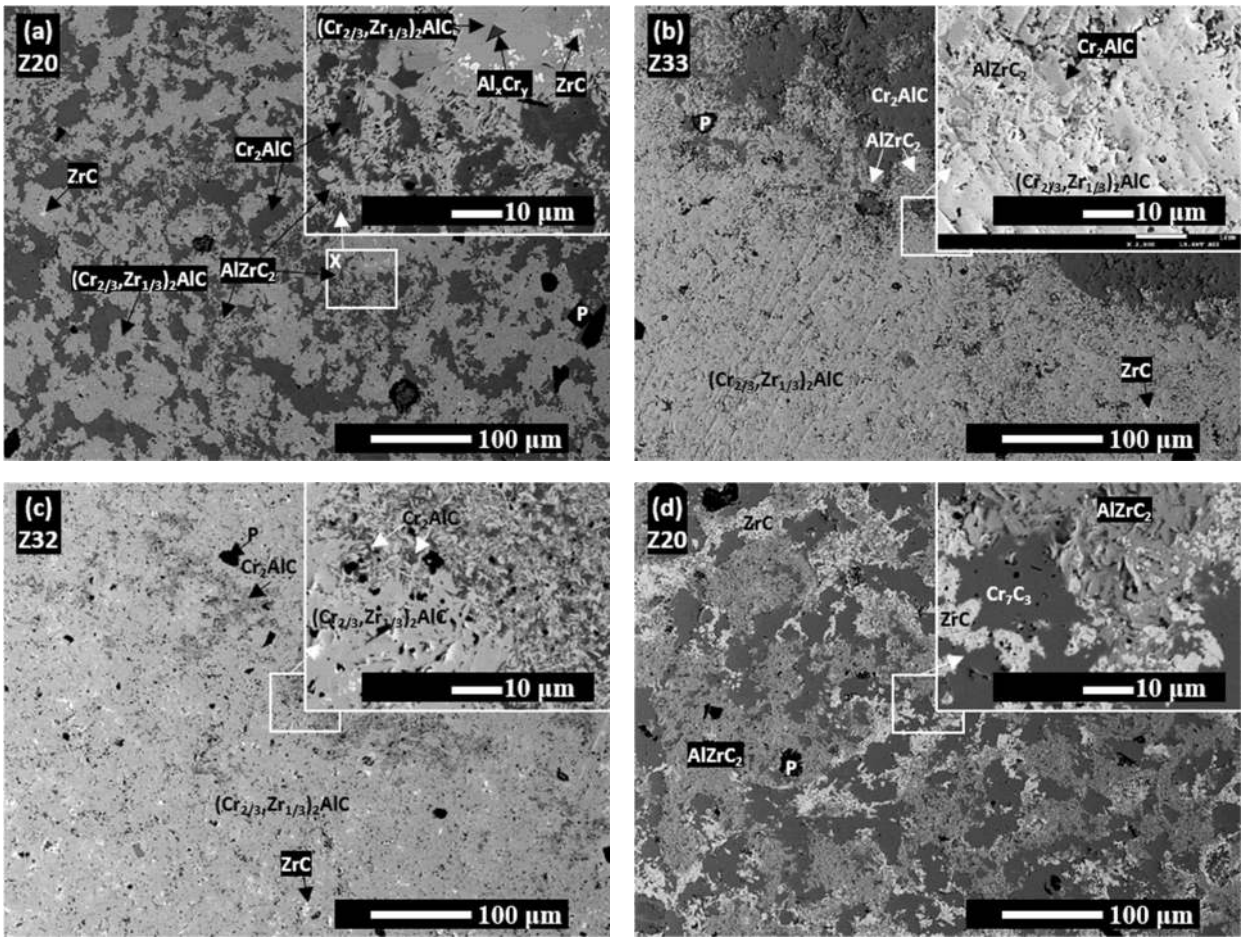

Fig. 4. Backscattered electron (BSE) images of (a) Z20, (b) Z33 and (c) Z32 ceramics after hot pressing for 30 min at 1300°C, and (d) Z20 ceramic hot pressed for 30 min at 1400°C. The inset images show the selected areas at a higher magnification.

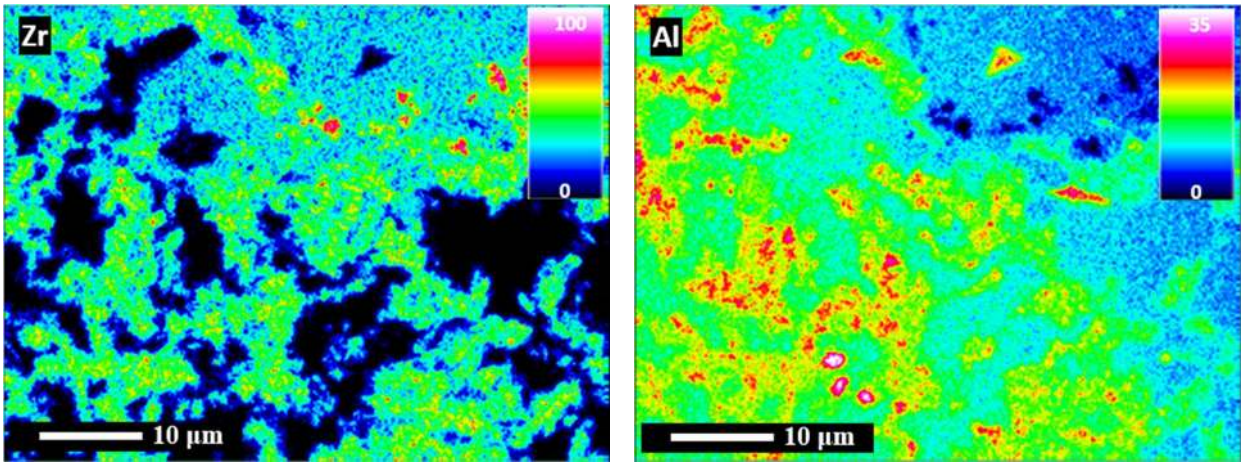

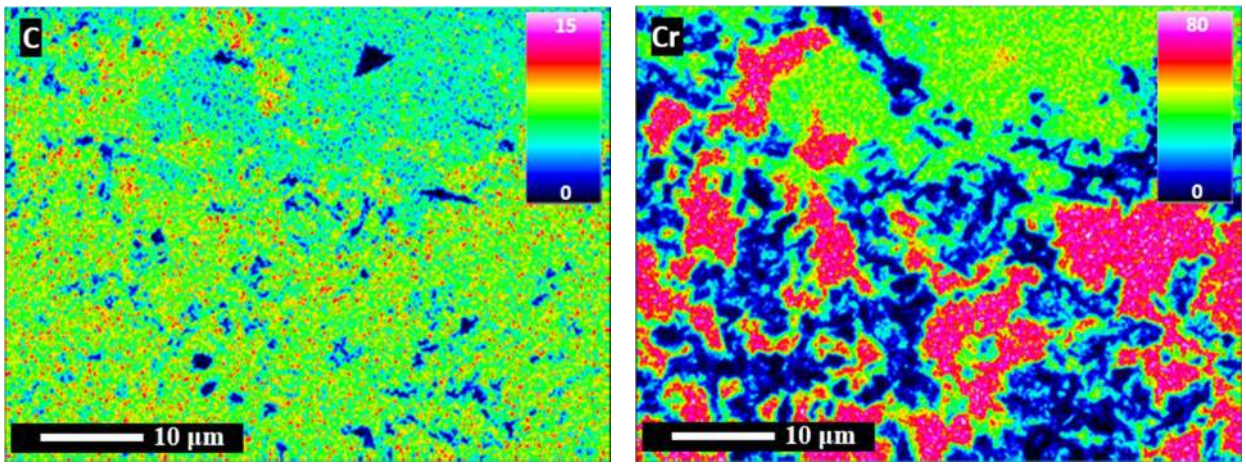

Fig. 5. EPMA elemental mapping of the marked area 'X' in Fig. 4(a) of the Z20 ceramic, showing the presence of the $(Cr_{2/3}Zr_{1/3})_2AlC$ and Cr_2AlC MAX phases, $AlZrC_2$, ZrC and Cr_xAl_y intermetallics.

Compositional analysis of the $(Cr_{2/3}Zr_{1/3})_2AlC$ phase was determined by quantitative EPMA-WDS. More than ten point analysis measurements were carried out at different locations on $(Cr_{2/3}Zr_{1/3})_2AlC$ grains with a size larger than 100 µm. The measured chemical composition shown in Table 3, corresponds to a (Cr+Zr):Al:C atomic ratio of 2.06:1:1.01 and that of Cr:Zr is 2.11:1. It can therefore be concluded that a new compound with the nominal chemical formula $(Cr_{2/3}Zr_{1/3})_2AlC$ was effectively synthesized. Note in Table 3 that the $(Cr_{2/3}Zr_{1/3})_2AlC$ *i*-MAX phase has a higher Cr/Zr atomic ratio of 2.06 than the stoichiometric ratio of 2. Most probably, the slightly decreased ZrH_2 content in Z32 favors the yield of the $(Cr_{2/3}Zr_{1/3})_2AlC$ *i*-MAX phase (Fig. 2b).

Table 3. The chemical composition of the $(Cr_{2/3}Zr_{1/3})_2AlC$ MAX phase, as-determined by EPMA-WDS (atomic %).

Sample No.	Cr	Zr	Al	C
Z20	34.4 ± 1.3	16.3 ± 0.6	24.6 ± 0.6	24.8 ± 0.9

The measured Vickers hardness of the Z32 ceramic after hot pressing at 1300°C is 11.11 ± 0.2 GPa. This value is comparable with that of $AlZrC_2$ (11.1 GPa)[37] but higher than for the Cr_2AlC MAX phase (5.2 GPa)[38] and other polycrystalline MAX phases (ranging from 2 GPa to 8 GPa)[1]. This is probably because of the different monoclinic structure of $(Cr_{2/3}Zr_{1/3})_2AlC$ phase. Scanning electron microscopy (SEM) images of a hardness indentation are illustrated in Fig. 6. Likewise most MAX phases, no radial crack was generated in the corners of the Vickers indentation (Fig. 6a). The characteristic rectangular, laminated MAX phase grains are visible for both the $(Cr_{2/3}Zr_{1/3})_2AlC$ and Cr_2AlC MAX phases in the area around the indent (Fig. 6b and 6c).

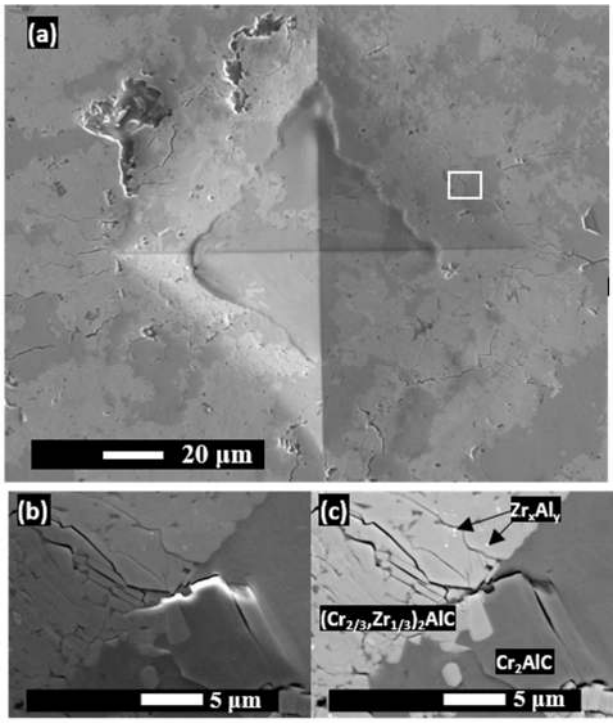

Fig. 6. (a) Secondary electron (SE) image of an indentation on the Z20 ceramic after hot pressing at 1300°C for 30min, and (b) SE and (c) BSE images of the selected zone in (a), showing the characteristic rectangular, laminated grains of the $(Cr_{2/3}Zr_{1/3})_2AlC$ and Cr_2AlC MAX phases. Zr_xAl_y = Zr-Al-Cr intermetallics.

Fig. 7 shows an overview scanning transmission electron microscopy (STEM) images of in-plane order for the $(Cr_{2/3}Zr_{1/3})_2AlC$ *i*-MAX phase and the schematic from two different crystallographic in-plane directions. Viewed along [110], the chemical order of Cr and Zr is evident in Fig. 7a. From the Z contrast, the bright spots corresponds to Zr while less bright spots corresponds to Cr. In-between each $(Cr_{2/3}Zr_{1/3})_2C$ layer, the Al atoms show a variation in their intensities (Fig. 7c). This is an effect of the Kagomé-like order within the Al layer which, when viewed along [110], have alternating columns of Al atoms with a 2:1 ratio[13]. The Kagomé pattern formed by Al atoms has been predicted by the theoretical calculation. The STEM image in Fig. 7 only indicates the Al columns along [110], which are not homogeneous. The columns close to Cr contain more Al atoms than those close to Zr. Further information and elaboration on this subject can be found in previous work by Dahlqvist et al.[13] When viewed along [100], Fig. 7b, there is a mixed contribution from both Cr and Zr and the phase looks the same as traditional MAX phases. From the analysis of STEM images and selected area electron diffraction (SAED) patterns, the crystal structure is monoclinic with a *C*2/*c* symmetry.

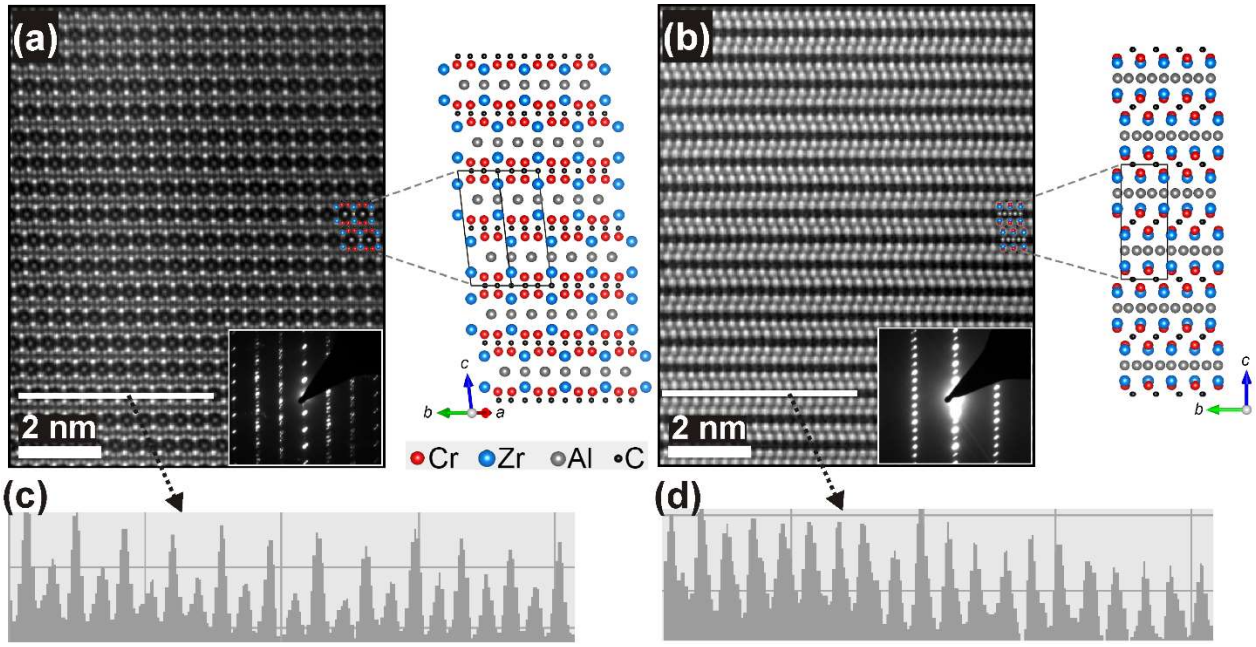

Fig. 7. STEM images of the Z33 ceramic hot pressed at 1300 °C and the corresponding schematic of $(Cr_{2/3}Zr_{1/3})_2AlC$ *i*-MAX phase in a monoclinic *C*2/*c* structure viewed along (a) [110] and (b) [100] zone axis, and with line scans (white lines in the images) across the Al layer viewed along (c) [100] and (d) [110] zone axis. The insert images are corresponding SAED patterns. Schematics were produced with VESTA[25].

The above results from XRD, EPMA-WDS, and STEM analysis confirm the successful synthesis of a new $(Cr_{2/3}Zr_{1/3})_2AlC$ MAX phase. STEM illustrates that $(Cr_{2/3}Zr_{1/3})_2AlC$ is a MAX phase-like compound. The formation mechanism of the $(Cr_{2/3}Zr_{1/3})_2AlC$ compound will be investigated in future work. Considering theoretical predictions, Shang *et al.* reported that $(Cr_{1-x},Zr_x)_2AlC$ phases with varying x were unstable at 0 K[10]. This exemplifies that the assumed crystal structure and order or disorder of, in this case, Cr and Zr atoms, has an impact on the corresponding result. The existence of this $(Cr_{2/3}Zr_{1/3})_2AlC$ *i*-MAX phase in the Cr-Zr-Al-C quaternary system might draw attention for both theoretical predictions and experimental synthesis.

Theoretical evaluation of magnetic ground state

Several Cr-based MAX phases have proven to be magnetic[39]. However, magnetic characterization requires as pure samples as possible. Since the ceramics with $(Cr_{2/3}Zr_{1/3})_2AlC$ contain secondary phases, like $AlZrC_2$, Cr_7C_3, $AlCr_2$, and Cr_2AlC, we here only probe magnetism using theory. Figure 8 shows the calculated energy difference ΔE_{NM} between different spin configurations relative to the non-magnetic (NM) state for $(Cr_{2/3}Zr_{1/3})_2AlC$ *i*-MAX phase through the PBE exchange-correlation functional (red bars). Only a few are found to be magnetic after relaxation, i.e., FM and A2, with a local moment around 0.03 to 0.23 μ_B per Cr atom, while most spin configurations relax to a

NM state. Note that ΔE_{NM} is rather small with lowest energy spin configuration being FM at -0.2 meV/atom. The small difference in ΔE_{NM} is also reflected in a small variation in their crystal structure. Detailed information on structural and magnetic information is given in Table S2. One of the reasons why most spin configurations end up as NM could be related to the "diluted" Cr, as compared to the case of Cr_2AlC.

In theoretical work on magnetic MAX phases, mostly focused on Cr-based M_2AX phases, the need for use of DFT+U methods or not has been debated, see Section 2.1 in Ref.[39] for further details. We have previously shown that a moderate value of $U_{eff} = U - J = 1$ eV could be used for Cr_2AC (A = Al, Ga, Ge)[23]. Herein, we further explore magnetism in $(Cr_{2/3}Zr_{1/3})_2AlC$ using $U_{eff} = 1$ eV to investigate the effect of more localized 3d electrons on the crystal and magnetic structure. The blue bars in Figure 8 show ΔE_{NM} using PBE+U. All considered spin configurations are after relaxation still spin-polarized where the one of lowest energy are X2 at -16 meV/atom. (X2 corresponds to an antiferromagnetic state with the spin direction changing sign upon crossing an X layer) The localization of 3d electrons thus results in larger values of ΔE_{NM} as well as increased local moments, from 0.23 to 1.27 μ_B per Cr, and increased lattice parameters as compared to the PBE case. Detailed information of structural and magnetic information is given in Table S3.

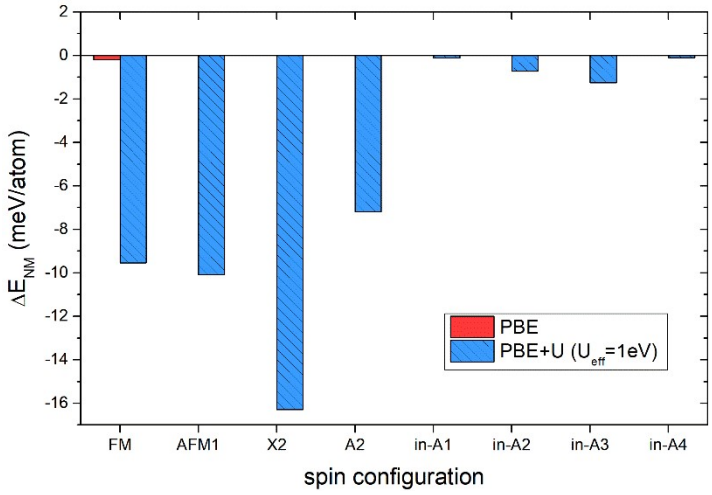

Fig. 8. Calculated energy difference ΔE_{NM} relative the non-magnetic (NM) solution for considered spin configurations of $(Cr_{2/3}Zr_{1/3})_2AlC$ using (a) PBE and (b) PBE+U with $U_{eff} = 1$ eV.

Conclusion

Guided by theoretical predictions, a new quaternary *i*-MAX phase with $(Cr_{2/3}Zr_{1/3})_2AlC$ composition was synthesized for the first time by hot pressing of Cr, ZrH_2, Al, and C mixtures at 1300°C. The chemical composition and crystal structure of $(Cr_{2/3}Zr_{1/3})_2AlC$ were identified by a combined characterization with EPMA-WDS, XRD, TEM, and SEM. The stacking sequence of $(Cr_{2/3}Ti_{1/3})_2C$ and Al layers results in a crystal structure of space group *C*2/*c*. *a*, *b*, and *c* lattice constants and angle β, which are determined by XRD analysis, are 9.0581 Å, 5.2263 Å, 13.2390 Å, and 103.2666°, respectively. The discovery of $(Cr_{2/3}Zr_{1/3})_2AlC$, along with other recent *i*-MAX phases, could be used as a case to reexamine other typical *i*-MAX compositions in established quaternary systems. Combined with theoretical calculations, it is possible to identify quaternary MAX phases candidates with either preferential in-plane order or with solid solution on the metal sites.

Supporting Information Available

Listings of Prototype structure, XRD patterns of starting powders, d-spacings and corresponding 2θ angles and magnetic information.

Acknowledgements

L.C. acknowledges the Research Fund of KU Leuven for offing the post-doctoral fellowship (PDM/16/140). The authors acknowledge the Hercules Foundation under Project ZW09-09 and AKUL/1319 (CombiS(T)EM). This research was partly funded by the PhD grant No. 131081 of T.L. of the Agency for Innovation by Science and Technology (IWT), Flanders, Belgium, partly by the European Atomic Energy Community's (Euratom) Seventh Framework Programme FP7/2007-2013 under grant agreement No. 604862 (FP7 MatISSE), and falls within the framework of the EERA (European Energy Research Alliance) Joint Programme on Nuclear Materials (JPNM). J.R. thanks support from the Swedish Foundation for Strategic Research (SSF) through the Synergy Grant FUNCASE and the Knut and Alice Wallenberg (KAW) Foundation for a Fellowship Grant, Project funding (KAW 2015.0043), and for support to the Linköping Ultra Electron Microscopy Laboratory. The Swedish Research council is gratefully acknowledged through Project 642-2013-8020. The theoretical calculations were carried out using supercomputer

resources which are provided by the Swedish National Infrastructure for Computing (SNIC) at the National Supercomputer Centre (NSC), the High Performance Computing Center North (HPC2N), and the PDC Center for High Performance Computing.

References

(1) Barsoum, M. W. *MAX Phases: Properties of Machinable Ternary Carbides and Nitrides*; Wiley-VCH Verlag GmbH & Co.: Berlin, 2013.

(2) Tallman, D. J.; Anasori, B.; Barsoum, M. W. A Critical Review of the Oxidation of Ti_2AlC, Ti_3AlC_2 and Cr_2AlC in Air. *Mater. Res. Lett.* **2016**, *3831* (January).

(3) Lapauw, T.; Halim, J.; Lu, J.; Cabioc'h, T.; Hultman, L.; Barsoum, M. W.; Lambrinou, K.; Vleugels, J. Synthesis of the Novel Zr_3AlC_2 MAX Phase. *J. Eur. Ceram. Soc.* **2016**, *36*, 943–947.

(4) Lapauw, T.; Lambrinou, K.; Cabioc'h, T.; Halim, J.; Lu, J.; Pesach, A.; Rivin, O.; Ozeri, O.; Caspi, E. N.; Hultman, L.; Eklund, P.; Rosen, J.; Barsoum, M. W.; Vleugels, J. Synthesis of the New MAX Phase Zr_2AlC. *J. Eur. Ceram. Soc.* **2016**, *36*, 1847–1853.

(5) Horlait, D.; Grasso, S.; Chroneos, A.; Lee, W. E. Attempts to Synthesise Quaternary MAX Phases $(Zr,M)_2AlC$ and $Zr_2(Al,A)C$ as a Way to Approach Zr_2AlC. *Mater. Res. Lett.* **2016**, *4*, 137–144.

(6) He, L. F.; Bao, Y. W.; Li, M. S.; Wang, J. Y.; Zhou, Y. C. Oxidation of $Zr_2[Al(Si)]_4C_5$ and $Zr_3[Al(Si)]_4C_6$ in Air. *J. Mater. Res.* **2008**, *23*, 3339–3346.

(7) He, L. F.; Lin, Z. J.; Bao, Y. W.; Li, M. S.; Wang, J. Y.; Zhou, Y. C. Isothermal Oxidation of Bulk $Zr_2Al_3C_4$ at 500 to 1000 °C in Air. *J. Mater. Res.* **2011**, *23*, 359–366.

(8) Lu, X.; Xiang, H.; He, L. F.; Sun, L.; Zhou, Y. Effect of Ti Dopant on the Mechanical Properties and Oxidation Behavior of $Zr_2[Al(Si)]_4C_5$ Ceramics. *J. Am. Ceram. Soc.* **2011**, *94*, 1872–1877.

(9) Tunca, B.; Lapauw, T.; Karakulina, O. M.; Batuk, M.; Cabioc, T. Synthesis of MAX Phases in the Zr-Ti-Al-C System. *Inorg. Chem.* **2017**, *56*, 3489–3498.

(10) Shang, L.; Music, D.; Baben, M. to; Schneider, J. M. Phase Stability Predictions of $Cr_{1-X},M_X)_2(Al_{1-Y},A_Y)(C_{1-Z},X_Z)$ (M = Ti, Hf, Zr; A = Si; X = B). *J. Phys. D. Appl. Phys.* **2014**, *47*, 65308.

(11) Tao, Q.; Dahlqvist, M.; Lu, J.; Kota, S.; Meshkian, R.; Halim, J.; Palisaitis, J.; Hultman, L.; Barsoum, M. W.; Persson, P. O. Å.; Rosen, J. Two-Dimensional $Mo_{1.33}C$ MXene with Divacancy Ordering Prepared from Parent 3D Laminate with in-Plane Chemical Ordering. *Nat. Commun.* **2017**, *8*, 1–7.

(12) Lu, J.; Thore, A.; Meshkian, R.; Tao, Q.; Hultman, L.; Rosen, J. Theoretical and Experimental Exploration of a Novel In-Plane Chemically Ordered $(Cr_{2/3}M_{1/3})_2AlC$ *i*-MAX Phase with M = Sc and Y. *Cryst. Growth Des.* **2017**, *17*, 5704–5711.

(13) Dahlqvist, M.; Lu, J.; Meshkian, R.; Tao, Q.; Hultman, L.; Rosen, J. Prediction and Synthesis of a Family of Atomic Laminate Phases with Kagomé-like and in-Plane Chemical Ordering. *Sci. Adv.* **2017**, *3*, 1–10.

(14) Kresse, G.; Hafner, J. Ab Initio Molecular Dynamics for Liquid Metals. *Phys. Rev. B* **1993**, *47*, 558–561.

(15) Kresse, G.; Furthmüller, J. Efficiency of Ab-Initio Total Energy Calculations for Metals and Semiconductors Using a Plane-Wave Basis Set. *Comput. Mater. Sci.* **1996**, *6*, 15–50.

(16) Kresse, G.; Furthmüller, J. Efficient Iterative Schemes for *Ab Initio* Total-Energy Calculations Using a Plane-Wave Basis Set. *Phys. Rev. B* **1996**, *54*, 11169–11186.

(17) Blöchl, P. E. Projector Augmented-Wave Method. *Phys. Rev. B* **1994**, *50*, 17953–17979.

(18) Kresse, G.; Joubert, D. From Ultrasoft Pseudopotentials to the Projector Augmented-Wave Method. *Phys. Rev. B* **1999**, *59*, 1758–1775.

(19) Perdew, J. P.; Burke, K.; Ernzerhof, M. Generalized Gradient Approximation Made Simple. *Phys. Rev. Lett.* **1996**, *77*, 3865–3868.

(20) Pack, J. D.; Monkhorst, H. J. Special Points for Brillouin-Zone Integrations. *Phys. Rev. B* **1976**, *13*, 5188–5192.

(21) Dudarev, S. L.; Botton, G. A.; Savrasov, S. Y.; Humphreys, C. J.; Sutton, A. P. Electron-Energy-Loss Spectra and the Structural Stability of Nickel Oxide: An LSDA+U Study. *Phys. Rev. B* **1998**, *57* , 1505–1509.

(22) Dahlqvist, M.; Alling, B.; Rosén, J. Correlation between Magnetic State and Bulk Modulus of Cr_2AlC. *J. Appl. Phys.* **2013**, *113*, 216103.

(23) Dahlqvist, M.; Alling, B.; Rosen, J. A Critical Evaluation of GGA + *U* Modeling for Atomic, Electronic and Magnetic Structure of Cr_2AlC, Cr_2GaC and Cr_2GeC. *J. Phys. Condens. Matter* **2015**, *27*, 95601.

(24) Dahlqvist, M.; Ingason, A. S.; Alling, B.; Magnus, F.; Thore, A.; Petruhins, A.; Mockute, A.; Arnalds, U. B.; Sahlberg, M.; Hjörvarsson, B.; Abrikosov, I. A.; Rosen, J. Magnetically Driven Anisotropic Structural Changes in the Atomic Laminate M n2GaC. *Phys. Rev. B* **2016**, *93*, 1–9.

(25) Momma, K.; Izumi, F. VESTA 3 for Three-Dimensional Visualization of Crystal, Volumetric and Morphology Data. *J. Appl. Crystallogr.* **2011**, *44*, 1272–1276.

(26) Dahlqvist, M.; Alling, B.; Abrikosov, I. A.; Rosén, J. Phase Stability of Ti_2AlC upon Oxygen Incorporation: A First-Principles Investigation. *Phys. Rev. B - Condens. Matter Mater. Phys.* **2010**, *81*, 1–8.

(27) Dahlqvist, M.; Alling, B.; Rosén, J. Stability Trends of MAX Phases from First Principles. *Phys. Rev. B - Condens. Matter Mater. Phys.* **2010**, *81*, 1–4.

(28) Thore, A.; Dahlqvist, M.; Alling, B.; Rosén, J. Temperature Dependent Phase Stability of Nanolaminated Ternaries from First-Principles Calculations. *Comput. Mater. Sci.* **2014**, *91*, 251–257.

(29) Ingason, A. S.; Petruhins, A.; Dahlqvist, M.; Magnus, F.; Mockute, A.; Alling, B.; Hultman, L.; Abrikosov, I. A.; Persson, P. O. Å.; Rosen, J. A Nanolaminated Magnetic Phase: Mn_2GaC. *Mater. Res. Lett.* **2017**, *2*, 89–93.

(30) Eklund, P.; Dahlqvist, M.; Tengstrand, O.; Hultman, L.; Lu, J.; Nedfors, N.; Jansson, U.; Rosén, J. Discovery of the Ternary Nanolaminated Compound Nb_2GeC by a Systematic Theoretical-Experimental Approach. *Phys. Rev. Lett.* **2012**, *109*, 2–5.

(31) Zunger, A.; Wei, S. H.; Ferreira, L. G.; J.E., B. Special Quasirandom Structures. *Phys. Rev. Lett.* **1990**, *65*, 353–356.

(32) Lutterotti, L.; Matthies, S.; Wenk, H. R. MAUD: A Friendly Java Program for Material Analysis Using Diffraction. *IUCr Newsl. CPD* **1999**, *21*, 14–15.

(33) Kraus, W.; Nolze, G. POWDER CELL - A Program for the Representation and Manipulation of Crystal Structures and Calculation of the Resulting X-Ray Powder Patterns. *J. Appl. Crystallogr.* **1996**, *29*, 301–303.

(34) Dahlqvist, M.; Rosen, J. Order and Disorder in Quaternary Atomic Laminates from First-Principles Calculations. *Phys. Chem. Chem. Phys.* **2015**, *17*, 31810–31821.

(35) He, L. F.; Zhou, Y. C.; Bao, Y. W.; Wang, J. Y.; Li, M. S. Synthesis and Oxidation of $Zr_3Al_3C_5$ Powders. *Int. J. Mater. Res.* **2007**, *98*, 3–9.

(36) Leela-Adisorn, U.; Choi, S. M.; Matsunaga, T.; Hashimoto, S.; Honda, S.; Hayakawa, K.; Awaji, H.; Yamaguchi, A. $AlZrC_2$ Synthesis. *Ceram. Int.* **2006**, *32*, 431–439.

(37) Leela-Adisorn, U.; Choi, S.-M.; Tera, N.; Takeuchi, T.; Hashimoto, S.; Honda, S.; Awaji, H.; Hayakawa, K.; Yamaguchi, A. Sintering and Mechanical Properties of $AlZrC_2$. *J. Ceram. Soc. Jpn.* **2005**, *113*, 188–190.

(38) Tian, W.; Wang, P.; Zhang, G.; Kan, Y.; Li, Y. Mechanical Properties of Cr_2AlC Ceramics. *J. Am. Ceram. Soc.* **2007**, *90*, 1663–1666.

(39) Ingason, A. S.; Dahlqvist, M.; Rosen, J. Magnetic MAX Phases from Theory and Experiments; A Review. *J. Phys. Condens. Matter* **2016**, *28*, 433003.

For Table of Contents only

SYNOPSIS

$(Cr_{2/3}Zr_{1/3})_2AlC$ *i*-MAX phase was theroticaly predicted and experimentally synthesised. This is the first report on synthesis of $(Cr_{2/3}Zr_{1/3})_2AlC$ *i*-MAX phase.

GRAPHICAL ABSTRACT